HOKKAIDO UNIVERSITY

Title	Motion and Morphology of Triple Junction in Peritectic Reaction Analyzed by Quantitative Phase-field Model
Author(s)	Ohno, Munekazu; Matsuura, Kiyotaka
Citation	ISIJ International, 50(12), 1879-1885 https://doi.org/10.2355/isijinternational.50.1879
Issue Date	2010-12-15
Doc URL	https://hdl.handle.net/2115/75419
Rights	著作権は日本鉄鋼協会にある
Type	journal article
File Information	ISIJ Int. 50(12)_ 1879-1885 (2010).pdf



Hokkaido University Collection of Scholarly and Academic Papers : HUSCAP

ISIJ International, Vol. 50 (2010), No. 12, pp. 1879–1885

Motion and Morphology of Triple Junction in Peritectic Reaction Analyzed by Quantitative Phase-field Model

Munekazu OHNO and Kiyotaka MATSUURA

Division of Materials Science and Engineering, Faculty of Engineering, Hokkaido University, Kita 13 Nishi 8, Kita-ku, Sapporo, Hokkaido 060-8628 Japan.

(*Received on April 20, 2010; accepted on June 18, 2010*)

Motion and morphology of triple junction during peritectic reaction process is analyzed for a model alloy system based on a quantitative-phase-field simulation for two-phase solidification involving diffusion in the solid. It is demonstrated that the dominative process controlling the motion of the reaction front gradually changes from the solid–solid transformation to the secondary solid solidification as the moving velocity of solid–solid interface decreases. On the other hand, the local shape of the triple junction is mainly determined by the balance between the interfacial energies regardless of the difference in the moving velocity of solid–solid interface.

KEY WORDS: peritectic reaction; phase-field simulation; triple junction; solidification; phase transformation; solid diffusion.

1. Introduction

Peritectic solidification is one of the most commonly observed phenomena in practical alloy systems. The peritectic process is considered to proceed in two stages.[1,2] The first stage is "peritectic reaction" in which all three phases, liquid (L), primary solid (δ) and secondary solid (γ) are in contact with each other and the γ phase grows along the δ–L interfacial boundary, finally leaving a layer of γ phase between L and δ phases. The second stage is "peritectic transformation" in which the transformations of δ to γ and L to γ take place by the motions of γ–δ and γ–L interfaces.

The peritectic reaction is characterized by the motion of triple junction between L/γ/δ phases. Hillert proposed a geometrical shape for the peritectic reaction,[3] which is schematically illustrated in **Fig. 1**. He assumed that the contact angles between interfaces at the triple junction obey the thermodynamic equilibrium relation described by the Young's law. When the solid diffusion is negligible, the position of γ–δ interface is always located behind the triple junction. The combination of these conditions results in the geometrical shape shown in Fig. 1. In addition, Fredriksson and Nylén proposed that the shape shown in Fig. 1 can be realized by the diffusion process, since the solute atom rejected by the γ solidification will diffuse through the liquid to δ phase, contributing the melting of the δ phase[4] as indicated by the bold arrows in Fig. 1. It is to be noted in Fig. 1 that the front edge of growing γ phase corresponds not to the triple junction but to γ–L interface. Then, the peritectic reaction proceeds only by the γ solidification. Based on this assumption, Fredriksson and Nylén applied the theoretical model developed by Bosze and Trivedi for describing the growth process of single phase in a matrix[5] to the analysis on the peritectic reaction process.[4] This model, which is called FN model hereafter, has been widely used for the analyses on the peritectic reaction process in several alloy systems.[6–10] It should be pointed out that the comparison between experimentally observed reaction rate and the FN model demonstrated that the reaction rate described by the FN model is fairly lower than the experimentally observed rate in several alloy systems.[6,7,10] It is noticed that the validity of the Hillert's assumption for the shape illustrated in Fig. 1 has not been well substantiated yet and the morphology of phases near the triple junction remains to be scrutinized in the cases of the different cooling conditions and different values of physical parameters.

Phase-field model has been developed as one of the powerful computational tools to describe the microstructural evolution process in phase transformation phenomena.[11–16] Of particular importance in this study is the recent development of the model based on thin-interface limit.[17,18] This

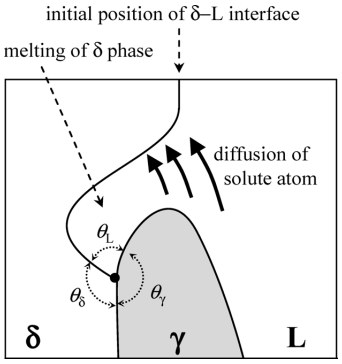


Fig. 1. Schematic illustration of peritectic reaction process proposed in Refs. 3,4).

© 2010 ISIJ

model is called the quantitative phase-field model in the light of the fact that it enables a quantitatively accurate simulation of microstructural process under a given set of physical parameters. The key to the quantitative phase-field modeling for an alloy system is the introduction of additional solute current termed the antitrapping current into the diffusion equation,[18] owing to which anomalous interface effects involved in the conventional model can be appropriately removed. While the originally developed antitrapping current scheme was applicable only to the single phase solidification in a binary alloy without the solid diffusion, this scheme was extended to the single phase solidification in multi-component alloys without the solid diffusion[19] and the single phase solidification in binary alloys with arbitrary value of the solid diffusivity.[20] Moreover, it was extended to the case of two-phase solidification in binary alloy.[21] The analysis on the peritectic reaction process requires the model for two-phase solidification. However, the available quantitative phase-field model in Ref. 21) is applicable only to the system in which the diffusion in solid is negligible and all the interfacial energies take the same value. The peritectic reaction generally involves the migration of solid–solid interface controlled by the solid diffusion and the interfacial energies are different for different interfaces in reality.

For the analysis on the peritectic reaction, the present authors recently developed a quantitative phase-field model for two-phase solidification process involving the solid diffusion in a binary alloy system with unequal interfacial energies.[22] It was demonstrated that this model yields the unique outcome with a finite value of the interface thickness. Hence, one can carry out a quantitatively accurate simulation as long as reliable values are available for the physical input parameters. Utilizing this model, then, the authors analyzed the peritectic reaction in carbon steel. It was demonstrated that the geometrical shape shown in Fig. 1 is not realized in the carbon steel and, therefore, the FN model is not validated.[23]

The geometrical shape near the triple junction and thus the peritectic reaction rate should depend on the diffusion processes in three phases. However, there is no detailed knowledge available regarding the dependencies of the shape of the triple junction and the reaction rate on the physical quantities such as the partition coefficient and diffusion coefficient. In particular, it has not been demonstrated by the experimental and theoretical works that the shape shown in Fig. 1 can be realized only by the solute diffusion process. In this study, these points are addressed by means of the quantitative phase-field simulation. Focusing on a model alloy system, we investigate the dependencies of the shape of the triple junction and the reaction rate on the partition coefficient and solid diffusivities. It will be seen that the dominative process controlling the motion of the reaction front gradually changes from the solid–solid transformation to the secondary solid solidification by decreasing the moving velocity of solid–solid interface. On the other hand, the local shape of the triple junction is mainly determined by the balance between the interfacial energies regardless of the difference in the moving velocity of the solid–solid interface.

2. Phase-field Model

The multi-phase-field models were developed to describe multi-phase solidification processes such as eutectic and peritectic reaction processes.[14–16] However, the conventional models generally involve the problems associated with several anomalous interface effects and the unexpected stabilization of an extra phase inside the interface,[21] thereby yielding the quantitatively inaccurate outcome. The quantitative phase-field model was developed for the two-phase solidification process in binary alloy system without the solid diffusion and with equal interfacial energies.[21] We recently extended that model to the case of arbitrary values of the solid diffusivities and interfacial energies,[22] which can be utilized to accurately describe the peritectic reaction process. In this section, we briefly explain about only the essential formulas of the quantitative phase-field model developed in Ref. 22).

During the peritectic reaction in a binary alloy system, there exist three phases, L, δ and γ phases. The existence of these phases is described by phase field, p_i, with i=L, δ and γ, each of which represents the probability of finding the corresponding phase. These phase fields should satisfy the following normalization condition,

$$\sum_i p_i = 1 \quad \text{.....(1)}$$

The summation is carried out over i=L, δ and γ. In addition to p_i, for convenience, we use the notation p_j and p_k to distinguish the different phases. Following Kim, Kim, Suzuki's (KKS) model,[13] the solute concentration, c, is described by mixture rule, $c=\sum c_i p_i$, with the concentration in i phase, c_i. Then, the time evolution of phase field, p_i, is described by the following equation,[22]

$$\begin{aligned}&\frac{1}{M(\{p_i\})}\frac{\partial p_i}{\partial t}\\&=\sum_k m_k\left(\frac{1}{2}\varepsilon^2\nabla^2 p_k - 2\omega(\{p_i\})p_k(1-p_k)(1-2p_k)\right.\\&\left.-\frac{\partial\omega(\{p_i\})}{\partial p_k}\left(\sum_j p_j^2(1-p_j)^2\right)-\sum_j\frac{\partial g_j}{\partial p_k}(f_j-\mu_c c_j)\right)\end{aligned} \quad \text{.....(2)}$$

$M(\{p_i\})$ is a mobility given as $M(\{p_i\})=2(\sum^* M_{ij}p_i p_j)(\sum^* p_i p_j)^{-1}$ where $\sum^*$ denotes the summation over $(i,j)=(\delta,\mathrm{L}),(\gamma,\mathrm{L}),(\gamma,\delta)$ and M_{ij} is the mobility for i–j interface as explicitly described later. m_k is a constant given as $m_k=-2/3$ with $k=i$ and $m_k=1/3$ with $k\neq i$. ε is the gradient energy coefficient and it is noted that this coefficient is not dependent on the type of interface in the present model. $\omega(\{p_i\})$ determines the contribution of double well potential and it is given as,[22]

$$\begin{aligned}&\omega(\{p_i\})\\&=\left(2\sum{}^* p_i^2 p_j^2\right)^{-1}\left(2\sum{}^*\omega_{ij}p_i^2p_j^2+\omega_{\mathrm{tri}}(p_ip_jp_k)^n\right)\end{aligned} \quad \text{.....(3)}$$

where the exponent n is larger than 1 and ω_{ij} indicates the

© 2010 ISIJ

potential height for i–j interface and ω_{tri} controls the potential height for mixture state of three phases. In Eq. (2), g_j is the interpolating function defined as $g_j(\{p_j\})=(p_j^2/4)\{15(1-p_j)[1+p_j-(p_k-p_i)^2]+p_j(9p_j^2-5)\}$.[21] f_j is the free energy density for bulk j phase and μ_c is the chemical potential. Note that in the derivation of Eq. (2), the condition for equal chemical potential, $\mu_c=\partial f_i/\partial c_i=\partial f_j/\partial c_j=\partial f_k/\partial c_k$, is introduced as is done in the KKS model.[13] The last term in the parenthesis of Eq. (2) corresponds to the thermodynamic driving force. This term can be approximated within the dilute solid solution limit as $f_j-\mu_c c_j\approx v_m^{-1}RT(-c_{k,e}^j+c_{j,e}^k-c_j)$ where v_m is the molar volume and R is the gas constant and $c_{j,e}^k$ is the equilibrium concentration in j phase in equilibrium with k phase. In this expression, k phase corresponds to a reference phase which was chosen to be liquid phase in our numerical computation. $c_{L,e}^L$ is given as $c_{L,e}^L=0$. Then, for example, the thermodynamic driving force for i–j interface is described as

$$f_j-f_i-\mu_c(c_j-c_i)=-v_m^{-1}\cdot RT(1-k_{ij})(c_{i,e}^j-c_i) \quad \text{.....(4)}$$

This expression is equivalent to the corresponding term in the single phase solidification model.[20]

The time evolution of concentration field, c, is described by the following diffusion equation,[22]

$$\frac{\partial c}{\partial t}=\nabla\left(\sum_i D_i p_i\nabla c_i+2\sum{}^{*}(\mathbf{n}_i\cdot\mathbf{n}_j)a_{ij}\frac{\varepsilon}{\sqrt{\omega_{ij}}}(c_j-c_i)\frac{\partial p_i}{\partial t}\mathbf{n}_i\right) \quad \text{...(5)}$$

where $\mathbf{n}_i$ is given by $\mathbf{n}_i=-\nabla p_i/|\nabla p_i|$. a_{ij} is defined as,

$$a_{ij}=\frac{1}{2\sqrt{2}}(D_j-k_{ij}D_i)\left[1-\frac{1}{2}\left(1-k_{ij}\frac{D_i}{D_j}\right)\chi_{ij}\right] \quad \text{..(6)}$$

where k_{ij} is the partition coefficient given as $k_{ij}=c_i/c_j$ and χ_{ij} is a parameter controlling convergence behavior of the output with respect to the computational grid size. The second term in the parenthesis of Eq. (5) indicates the antitrapping current term which is required to eliminate the anomalous interface effects.

In the present model, the steady state profile of p_i for a planar i–j interface is described as

$$p_i=\frac{1}{2}\left(1-\tanh\left(\frac{x}{\sqrt{2}W_{ij}}\right)\right) \quad \text{.....(7)}$$

where $W_{ij}=\varepsilon/\omega_{ij}^{1/2}$. It is noted that W_{ij} corresponds to the measure of the i–j interface thickness. Also, the i–j interfacial energy, σ_{ij}, is represented by $\sigma_{ij}=\varepsilon(\omega_{ij})^{1/2}/(3\cdot 2^{1/2})$. Hence, when σ_{ij} and W_{ij} are given, ω_{ij} and ε are uniquely determined. Within the thin-interface limit, also, the following relation should be satisfied at the condition for vanishing linear kinetic coefficient,

$$M_{ij}=\left(\frac{15}{4}\frac{a_2\varepsilon^2RT_{m,ij}}{\omega_{ij}D_jv_m}(1-k_{ij})(c_{j,e}^i-c_{i,e}^j)\times\left[1-\frac{1}{2}\left(1-k_{ij}\frac{D_i}{D_j}\right)\chi_{ij}\right]\right)^{-1} \quad \text{.....(8)}$$

where $a_2=0.6276\cdots$ and $T_{m,ij}$ is the transition temperature between i and j phases at $c=0$.

In the present model, the solid diffusion is explicitly taken into account, which is of critical importance in analyzing the peritectic reaction process, and the inequality of interfacial energies can be dealt with. It should be noticed that the present model is free from the problem associated with the unexpected formation of extra phase inside the interface as discussed in Ref. 22). The formation of the extra phase can be successfully suppressed by the introduction of additional potential for mixture state of three phases in Eq. (3). The contribution of this additional potential is controlled by the values of n and ω_{tri} that turn out to be the parameters controlling the convergence behavior of the outcome with respect to the interface thickness.[22] The most important fact is that the present model is exactly reduced to the available thin-interface limit model for the single phase solidification developed in Ref. 20).

3. Computational Details

We solved the time evolution Eqs. (2) and (5) based on the standard second-order finite difference formula with the squire grid spacing, Δx. In all the calculations, the interface thicknesses were set to be $W_{\gamma\delta}=2.0\times\Delta x$, $W_{\delta\mathrm{L}}=\sigma_{\gamma\delta}W_{\gamma\delta}/\sigma_{\delta\mathrm{L}}$ and $W_{\gamma\mathrm{L}}=\sigma_{\gamma\delta}W_{\gamma\delta}/\sigma_{\gamma\mathrm{L}}$. Also, we employed $n=1.4$ and $\omega_{\mathrm{tri}}=\omega_{\delta\mathrm{L}}+\omega_{\gamma\mathrm{L}}+\omega_{\gamma\delta}$ in Eq. (3) and $\chi_{ij}=0$ in Eqs. (6) and (8) with which the present model yields well convergence behavior of the outcome with respect to W_{ij}.[22] The degree of undercooling from the peritectic temperature, ΔT, was set to be $\Delta T=10$ K in all the calculations.

The values of all the input parameters are summarized in **Table 1**. It is noted that these parameters correspond to those for the Fe–C system. In the present study, our focus is placed on the dependencies of the peritectic reaction and transformation processes on the values of the partition coefficient and solid diffusivities. The partition coefficient, $k_{\gamma\mathrm{L}}$, was fixed to be $k_{\gamma\mathrm{L}}=0.334$ and the relation, $k_{\gamma\delta}=k_{\gamma\mathrm{L}}/k_{\delta\mathrm{L}}$, is held. The partition coefficient $k_{\gamma\delta}$ was varied from 1.34 to 6.68, which leads to the variation of $k_{\delta\mathrm{L}}$ from

Table 1. Values of physical parameters used in the present study.

Quantity	Symbol	Value used
Molar volume	v_m	7.7×10^{-6} m^3/mol
Melting temperature of pure bcc-Fe	$T_{m,\delta\mathrm{L}}$	1811 K
Melting temperature of pure fcc-Fe	$T_{m,\gamma\mathrm{L}}$	1801 K
δ/γ transition temperature of pure Fe	$T_{m,\gamma\delta}$	1399 K
Liquidus slope of δ phase	m_δ	1828 K/mol fraction
Liquidus slope of γ phase	m_γ	1399 K/mol fraction
Interfacial energy of δ-L boundary	$\sigma_{\delta\mathrm{L}}$	0.204 J/m^2
Interfacial energy of γ-L boundary	$\sigma_{\gamma\mathrm{L}}$	0.319 J/m^2
Interfacial energy of γ-δ boundary	$\sigma_{\delta\gamma}$	0.370 J/m^2

© 2010 ISIJ

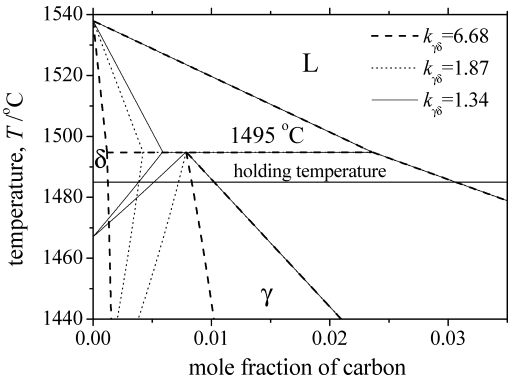


Fig. 2. Phase diagram calculated by using the physical parameters listed in Table 1 and the different values of $k_{\gamma\delta}$.

0.25 to 0.05. It is noted that the value of $k_{\delta L}$ is not relevant to the motion of γ–L and γ–δ interfaces, while the different value of $k_{\gamma\delta}$ will yield appreciable difference in the motion of γ–δ interface. **Figure 2** shows the phase diagram in this binary system calculated using the parameters listed in Table 1 and the different values of $k_{\gamma\delta}$. The diffusion coefficient in liquid phase, D_L, was fixed to be $D_L=2.0\times10^{-8}$ m^2/s. The diffusion coefficients, D_δ and D_γ, were given as $D_\delta=q_\delta.D_\delta^i$ and $D_\gamma=q_\gamma.D_\gamma^i$ with $D_\delta^i=4.0\times10^{-9}$ and $D_\gamma^i=6.0\times10^{-10}$ m^2/s for convenience. The constants, q_δ and q_γ, were varied from 1.0 to 1.0×10^{-3}.

We first carried out the one-dimensional simulation for the isothermal peritectic transformation. The system initially consists of the liquid phase with $c_{L,e}^{\delta}=2.90\times10^{-2}$ and δ phase with $c_{\delta,e}^{L}=5.19\times10^{-3}$ and γ phase with $c_{\gamma,e}^{L}=1.02\times10^{-2}$ between the liquid and δ phases. The initial thickness of γ phase is 2.5×10^{-7} m. The computational grid size, Δx, is $\Delta x=5.0\times10^{-8}$ m. The total length of the system is 60 μm which is large enough to avoid the effect of the system size on the motions of the interfaces. The zero flux boundary conditions for p_i and c were employed at both edges of the system. After the concentration profile was relaxed by holing at a given temperature for a certain period, the moving distances of γ–δ and γ–L planar interfaces were calculated. From this one-dimensional analysis, the moving velocities of γ–δ and γ–L planar interfaces can be calculated and these results are utilized in the discussion for the peritectic reaction process.

For the analysis on isothermal peritectic reaction process, we used the two-dimensional system in which there are δ phase with $c_{\delta,e}^{L}$ and liquid phase with $c_{L,e}^{\delta}$ and the δ–L interface forms along y direction at the origin of x axis. Also, a semicircular γ phase with a radius r_γ exists and the center of this circle is located at the origins of x and y axes. Then, the γ phase grows along the δ–L interface (y direction) and the velocity of the front edge of growing γ phase, *viz.*, the peritectic reaction rate was calculated. In all the two-dimensional simulations, we employed $r_\gamma=20\times10^{-8}$ m, $\Delta x=1.0\times10^{-8}$ m and $\Delta t=1.0\times10^{-10}$ s. We employed the zero flux boundary conditions for p_i and c along all the boundaries of the system. The system size was characterized by the total lengths of x and y axes, W_x and W_y. As pointed out in Ref. 22), the steady state velocity of the peritectic reaction is sensitive to system size. It is necessary for the analysis on the steady state behavior to employ a system size which is sufficiently large to avoid such a size effect. Our preliminary calculations showed that it is computationally demanding to employ sufficiently large system in some cases. In this study, we used $W_x=4$ μm and $W_y=3$ μm in all the calculations. Hence, some results especially in the case of low solid diffusivity do not precisely represent the steady state behavior of the reaction. However, it does not essentially alter our discussion.

4. Results and Discussion

4.1. Dependency on Partition Coefficient between γ and δ Phases

Figure 3(a) shows the concentration profiles obtained by one-dimensional simulation for isothermal peritectic transformation. The values of q_δ and q_γ were set to be $q_\delta=q_\gamma=1.0$ and the partition coefficient was $k_{\gamma\delta}=1.87$. These values are quite close to those at $\Delta T=10$ K in the Fe–C system. The origin of the spatial axis corresponds to the initial position of γ–L interface. The γ–L and γ–δ interfaces move to the left-hand and right-hand sides, respectively. As mentioned in the previous section, the moving distances of the interfaces were calculated after the system was relaxed for a certain period and therefore, the thickness of γ phase at $t=0.0$ is larger than the initial thickness, 2.5×10^{-7} m in Fig. 3(a). The moving distance of i–j interface, x_{ij}, is plotted with respect to the square root of time in Fig. 3(b). It is important to note that the γ–δ interface migrates at a velocity much higher than the γ–L interface, which is because the concentration difference at γ–δ interface is much smaller than that at γ–L interface. In Fig. 3(b), the increase in the moving distance of each interface obeys the parabolic growth law described by $x_{ij}=a_{ij}t^{1/2}$ with the parabolic rate constant, a_{ij}. The one-dimensional calculations were performed with the different values of $k_{\gamma\delta}$ and the calculated value of a_{ij} is shown in **Fig. 4**. The rate constant $a_{\gamma L}$ takes almost the constant value, while $a_{\gamma\delta}$ substantially decreases with the increase in $k_{\gamma\delta}$, finally being less than $a_{\gamma L}$ at $k_{\gamma\delta}=6.68$. This is ascribable to the fact that the increase in $k_{\gamma\delta}$ yields the increase in the concentration difference at γ–δ interface, while the value of $k_{\gamma\delta}$ is irrelevant to the concentration difference at γ–L interface. The increased concentration difference at the γ–δ interface requires a larger amount of solute to diffuse for δ-to-γ transformation at the interface, leading to a shorter migration distance of the γ–δ interface.

Shown in **Fig. 5** is the peritectic reaction rate, *viz.*, the velocity of the front edge of growing γ phase along the δ–L interface calculated with different values of $k_{\gamma\delta}$ in the two-dimensional system. The values of q_δ and q_γ were set to be $q_\delta=q_\gamma=1.0$. It is seen that the peritectic reaction rate significantly decreases with the increase in $k_{\gamma\delta}$. As discussed above, the variation in $k_{\gamma\delta}$ leads to the difference in the moving velocity of only γ–δ interface. Therefore, the decrement of the reaction rate essentially originates from slowing of the γ–δ interfacial migration due to the large concentration difference at γ–δ interface.

Figure 6 shows the morphology of phases near the triple junction during the peritectic reaction calculated with the different values of $k_{\gamma\delta}$. These lines represent level 0.5 contour lines of phase fields. The origin of x axis corresponds

© 2010 ISIJ

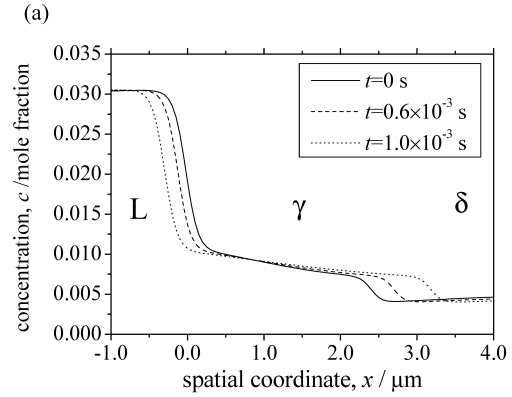


Fig. 3. (a) Concentration profile during isothermal peritectic transformation at $\Delta T=10$ K calculated with $q_\delta=q_\gamma=1$ and $k_{\gamma\delta}=1.87$. (b) Relation between the moving distance of each interface and the square root of time during the peritectic transformation process.

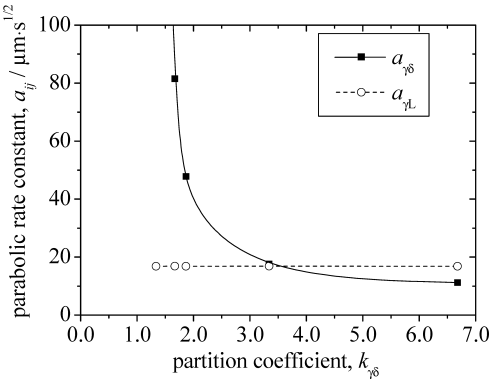


Fig. 4. Dependence of parabolic rate constant, a_{ij}, on partition coefficient, $k_{\gamma\delta}$.

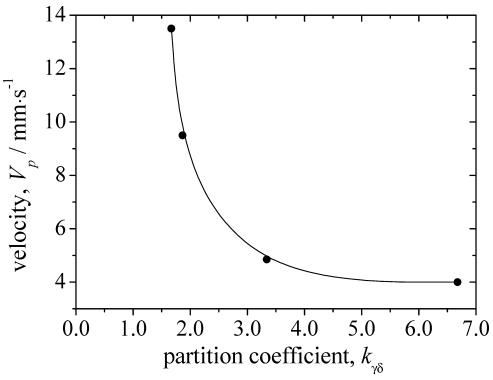


Fig. 5. Dependence of velocity of growing γ phase on partition coefficient, $k_{\gamma\delta}$, calculated with $q_\delta=q_\gamma=1$.

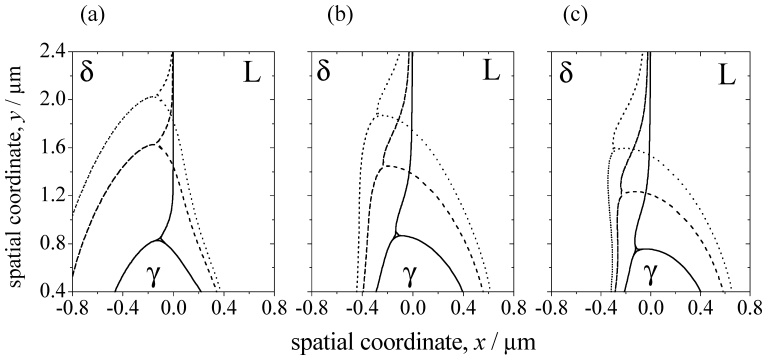


Fig. 6. Morphology of phases near triple junction calculated with (a) $k_{\gamma\delta}=1.67$, (b) $k_{\gamma\delta}=3.34$ and (c) $k_{\gamma\delta}=6.68$. In each figure, the solid, dashed and dotted lines represent level 0.5 contour lines of phase fields at t_1, t_2 and t_3, respectively. $t_1=0.6\times10^{-4}$, $t_2=1.2\times10^{-4}$, $t_3=1.5\times10^{-4}$ s in Fig. 6(a) and $t_1=1.2\times10^{-4}$, $t_2=2.4\times10^{-4}$, $t_3=3.0\times10^{-4}$ s in Figs. 6(b) and 6(c).

to the initial position of δ–L interface. The deviation of the triple junction position from the origin, $x=0$, indicates that the melting of δ phase occurs due to the enrichment of solute element in the liquid near the solidification front of γ phase. The melting of δ phase takes place in all the cases, while the morphology of phases near the triple junction is appreciably dependent on the value of $k_{\gamma\delta}$. Figure 6(a) shows that at $k_{\gamma\delta}=1.67$, the moving velocity of γ–δ interface is much faster than that of γ–L interface, as already shown in Fig. 4. In Fig. 6(a), the position of triple junction defined by $p_L=p_\delta=p_\gamma=1/3$ is slightly behind the front edge of γ–δ interface at each time period, although the difference between their positions may not be distinctly seen in the drawings. In other words, the front edge of growing γ phase always corresponds to γ–δ interface and the reaction proceeds by $\delta\rightarrow\gamma$ solid transformation at the reaction front. On the other hand, at $k_{\gamma\delta}=6.68$ (Fig. 6(c)), the migration of γ–δ interface is quite slow and the front edge of growing γ phase corresponds to the γ–L interface. These results indicate that the dominative process controlling the motion of the reaction front changes from $\delta\rightarrow\gamma$ solid transformation to γ solidification as the value of $k_{\gamma\delta}$ increases or the moving velocity of γ–δ interface decreases.

From a closer look at Fig. 6, it is realized that the local

© 2010 ISIJ

shape of the triple junction appears almost identical regardless of the different values of $k_{\gamma\delta}$. When the contact angle between i–j and i–k interfaces at the triple junction is denoted as θ_i, the equilibrium contact angles are calculated to be θ_L=92.9°, θ_δ=121.6° and θ_γ=146.0° based on the Young's law with the values of interfacial energies listed in Table 1. It was demonstrated in our previous report[23] that the present model reproduces these contact angles within the accuracy of less than 1° at ΔT=0.25 K. The precise determination of the contract angles in Fig. 6 is not possible, because each interface near the triple junction deviates from flat shape. Yet, the local shapes of the triple junction do not significantly differ from the equilibrium shapes in each case. Hence, it can be mentioned that the morphology of phases very close to the triple junction is mainly determined by the balance between the interfacial energies even though the moving velocities of the interfaces are different.

4.2. Dependency on Solid Diffusivities

We performed the one-dimensional simulations for isothermal peritectic transformation to investigate the dependence of the moving velocity of the interface on the diffusion coefficients. In all the calculations, we employed $k_{\gamma\delta}$=1.87. As mentioned, the solid diffusivities, D_δ and D_γ, are given as $D_\delta=q_\delta . D_\delta^i$ and $D_\gamma=q_\gamma . D_\gamma^i$, respectively, with $D_\delta^i=4.0\times10^{-9}$ and $D_\gamma^{\ i}=6.0\times10^{-10}$ m^2/s. We carried out three types of calculations. The first type is the calculations for a fixed value of q_γ=1.0 and different values of q_δ=1.0, 1.0×10^{-1}, 1.0×10^{-2} and the second type is those for a fixed value of q_δ=1.0 and the different values of q_γ=1.0, 1.0×10^{-1} and 1.0×10^{-2}. Furthermore, we performed the calculations for $q_\delta=q_\gamma$=1.0, 1.0×10^{-1}, 1.0×10^{-2} and 1.0×10^{-3}. The calculated parabolic rate constant is shown in **Fig. 7** where the vertical dotted line was drawn from each data point to the x–y plane for visual aid. It is seen that the rate constant of γ–L planar interface is almost irrelevant to the value of solid diffusivities. On the other hand, the rate constant of γ–δ interface appreciably decreases with the decreases in q_γ and q_δ. In particular, the motion of γ–δ interface is sensitive to the value of D_δ, compared with D_γ. As can be grasped from Fig. 3(a), a relatively large concentration gradient exists in the γ phase compared with that in the δ phase and, hence, the motion of each interface is not considerably affected by the value of D_γ. Most importantly, the parabolic rate constant for the γ–δ interface takes almost null value when $q_\delta=q_\gamma=1.0\times10^{-3}$. Hence, in this case, the γ–δ interface does not migrate and the peritectic transformation proceeds entirely by the γ solidification.

The dependence of the peritectic reaction rate on the solid diffusivities is shown in **Fig. 8**. The decrement of solid diffusivities leads to the reduction of the reaction rate. The influence of D_δ is more prominent compared with the case of D_γ as is consistent with the results of planar interface shown in Fig. 7. This is because the large concentration gradient exists in the γ phase and the diffusion process in the γ phase easily takes place even with low value of D_γ. As discussed above, the γ–δ planar interface does not migrate at $q_\delta=q_\gamma=1.0\times10^{-3}$ and, in this case, the peritectic reaction rate should be determined only by the γ solidification. This is, in fact, evident in the morphology of phases near the triple junction as discussed below.

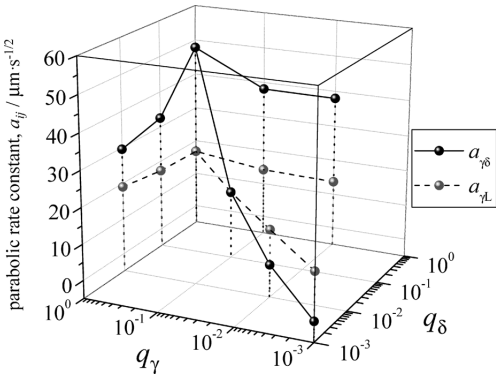


Fig. 7. Dependence of parabolic rate constant on the diffusion coefficient. The diffusion coefficients, D_δ and D_γ, were defined as $D_\delta=q_\delta . D_\delta^i$ and $D_\gamma=q_\gamma . D_\gamma^i$, respectively, with $D_\delta^i=4.0\times10^{-9}$ and $D_\gamma^{\ i}=6.0\times10^{-10}$ m^2/s.

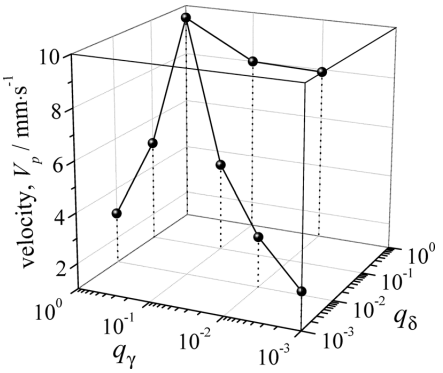


Fig. 8. Dependence of the peritectic reaction rate on diffusion coefficients.

Figure 9 demonstrates the morphology of phases near the triple junction calculated for the different values of q_δ and q_γ. It is noticed that the melting of δ phase takes place in all the cases, as can be realized from the deviation of the position of triple junction from x=0. The morphology of the phases is quite different depending on the solid diffusivities. In the case of $q_\delta=q_\gamma$=1.0 (Fig. 9(a)), the front edge of growing γ phase corresponds to the triple junction. This is also the case for q_δ=1.0 and $q_\gamma=1.0\times10^{-2}$ (Fig. 9(c)). However, when the diffusion coefficient in δ phase is reduced, the morphology of phases drastically changes as shown in Figs. 9(b) and 9(d). In these cases, the γ–δ interfacial velocity is quite small (Fig. 7) and the front edge of growing γ phase corresponds not to the triple junction but to the γ–L interface. Then, the growth of γ phase at the reaction front takes place mainly by the γ solidification.

In Fig. 9, the local shape of the triple junction does not significantly differ from the equilibrium contact angle described by the Young's law in all the cases. Hence, it is again shown that the morphology of phases very close to the triple junction is mainly determined by the balance between the interfacial energies even though the moving velocities of the interfaces are quite different.

It should be pointed out in Figs. 9(b) and 9(d) that the triple junction gradually moves to the left-hand side with the time and the amount of melting δ phase ahead of growing γ phase increases. This indicates that the results shown in Figs. 9(b) and 9(d) do not reach the steady state. When the reaction proceeds mainly by the γ solidification and the

© 2010 ISIJ

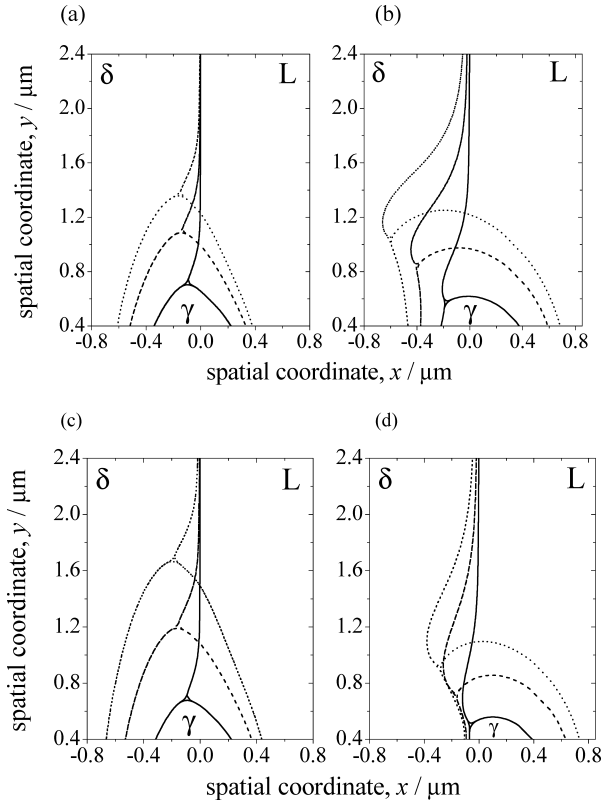


Fig. 9. Morphology of phases near triple junction calculated for (a) $q_\delta=1.0$ and $q_\gamma=1.0$, (b) $q_\delta=1.0\times10^{-2}$ and $q_\gamma=1.0$ (c) $q_\delta=1.0$ and $q_\gamma=1.0\times10^{-2}$ and (d) $q_\delta=q_\gamma=1.0\times10^{-3}$. In each figure, the solid, dashed and dotted lines represent level 0.5 contour lines of phase fields at t_1, t_2 and t_3, respectively. $t_1=0.4\times10^{-4}$, $t_2=0.8\times10^{-4}$, $t_3=1.0\times10^{-4}$ s in Fig. 9(a), $t_1=0.3\times10^{-4}$, $t_2=0.8\times10^{-4}$, $t_3=1.2\times10^{-4}$ s in Fig. 9(c) and $t_1=1.2\times10^{-4}$, $t_2=2.4\times10^{-4}$, $t_3=3.0\times10^{-4}$ s in Figs. 9(b) and 9(d).

reaction rate is low, the δ phase far from the reaction front melts due to the long diffusion length in the liquid associated with γ solidification. Therefore, the results for the low solid diffusivity in δ phase were prone to be affected by the system size. It was quite difficult to completely eliminate the effect of the system size in these cases even with the moving frame calculation. Since the results shown in Figs. 9(b) and 9(d) sufficiently represent the essential feature for our discussion, we do not further attempt to calculate the steady state in these cases.

As is seen in Figs. 6(b) and 6(c) and Figs. 9(b) and 9(d), when the moving velocity of δ–γ interface is quite small, the melting of δ phase substantially occurs and the growth of γ phase proceeds mainly by the γ solidification. In an extreme case, it may be allowed to assume that the peritectic reaction proceeds only by the γ solidification. However, this assumption is not validated in some systems such as the Fe–C system.[23] The present analysis showed that when the partition coefficient between the primary solid (δ) and secondary solid (γ) phases is not so large and/or the diffusion coefficient in the primary solid (δ) phase is not significantly smaller than that in the liquid phase, the contribution of solid diffusion in the peritectic reaction process is not negligible. Hence, the analysis on the peritectic reaction process essentially requires the effect of solid diffusion to be explicitly considered.

5. Conclusion

The motion and morphology of the peritectic triple junction were investigated for a model alloy system with the different solid diffusivities and partition coefficient by means of the quantitative phase-field simulation. It was demonstrated that the dominative process controlling the motion of the reaction front changes from the solid–solid transformation to the secondary solid solidification as the moving velocity of solid–solid interface decreases. On the other hand, the morphology of phases very close to the triple junction is mainly determined by the balance between the interfacial energies even though the moving velocities of the interfaces are quite different. When the migration of solid–solid interface is negligibly slow, the peritectic reaction proceeds only by the γ solidification and the classical theoretical model used by Fredriksson and Nylén may be validated. However, the analysis on the peritectic reaction process essentially requires the effect of solid diffusion to be explicitly considered.

Acknowledgments

This work is supported by 18th ISIJ Research Promotion Grant. The author M.O. acknowledges partial financial support from the Next Generation Super Computing Project, Nano-science Program, MEXT, Japan.

REFERENCES

1) H. W. Kerr, J. Cisse and G. F. Bolling: *Acta Mater.*, **22** (1974), 677.
2) H. Fredriksson: *Met. Sci.*, **10** (1976), 76.
3) M. Hillert: Solidification and Casting of Metals, The Metals Society, London, (1979).
4) H. Fredriksson and T. Nylén: *Met. Sci.*, **16** (1982), 283.
5) W. Bosze and R. Trivedi: *Metall. Trans.*, **5** (1974), 511.
6) H. Sibata, Y. Arai, M. Suzuki and T. Emi: *Metall. Mater. Trans.*, **31B** (2000), 981.
7) D. Phelan, M. Reid and R. Dippenaar: *Mater. Sci. Eng. A*, **477** (2008), 226.
8) D. M. Stefanescu: *ISIJ Int.*, **46** (2006), 786.
9) N. J. McDonald and S. Sridhar : *J. Mater. Sci.*, **40** (2005), 2411.
10) N. J. McDonald and S. Sridhar: *Metall. Mater. Trans.*, **34A** (2003), 1931.
11) A. Karma: Encyclopedia of Materials Science and Technology, Elsevier, Oxford, (2001).
12) I. Steinbach: *Modell. Simul. Mater. Sci. Eng.*, **17** (2009), 073001.
13) S. G. Kim, W. T. Kim and T. Suzuki: *Phys. Rev. E*, **60** (1999), 7186.
14) I. Steinbach, F. Pezzola, B. Nestler, M. Seeßelberg, R. Prieler, G. J. Schmitz and J. L. L. Rezende: *Physica D*, **94** (1996), 135.
15) I. Steinbach and F. Pezzola: *Physica D*, **134** (1999), 385.
16) S. G. Kim, W. T Kim, T. Suzuki and M. Ode: *J. Cryst. Growth*, **261** (2004), 135.
17) A. Karma and W.-J. Rappel: *Phys. Rev. E*, **57** (1998), 4323.
18) A. Karma: *Phys. Rev. Lett.*, **87** (2001), 115701.
19) S. G. Kim: *Acta Mater.*, **55** (2007), 4391.
20) M. Ohno and K. Matsuura: *Phys. Rev. E*, **79** (2009), 031603.
21) R. Folch and M. Plapp: *Phys. Rev. E*, **72** (2005), 011602.
22) M. Ohno and K. Matsuura: *Acta Mater.*, **58** (2010), 5749.
23) M. Ohno and K. Matsuura: *Acta Mater.*, **58** (2010), 6134.

© 2010 ISIJ